

Research Article

Numerical Investigation on the Dynamic Characteristics of an Adjustable Power Turbine Used in Environmental Control System

Qihang Lu ¹, Qi Zhang,² and Dalin Zhang ¹

¹College of Aerospace Engineering, Nanjing University of Aeronautics and Astronautics, Nanjing, China

²Aviation Industry Corporation of China, Nanjing Engineering Institute of Aircraft Systems, Nanjing, China

Correspondence should be addressed to Dalin Zhang; zhangdalin@nuaa.edu.cn

Received 6 July 2020; Revised 27 August 2020; Accepted 11 September 2020; Published 28 September 2020

Academic Editor: Zhihan Lv

Copyright © 2020 Qihang Lu et al. This is an open access article distributed under the Creative Commons Attribution License, which permits unrestricted use, distribution, and reproduction in any medium, provided the original work is properly cited.

In this paper, the environmental control system of aircraft driven by a power turbine is further analyzed. Through the numerical simulation of the change of the bleed state under different flight conditions and the change of the flow field under different nozzle opening, the simulation results are verified by the experimental results, and the specific change rules of the power turbine output torque, power, and bleed flow are obtained. It is analyzed quantitatively that adjusting the adjustable nozzle ring can keep the output power stable, widen the flight envelope, and improve the stability of the environmental control system.

1. Introduction

The main purpose of the aircraft environmental control system is to provide comfortable environmental conditions for airborne personnel and electronic equipment. By controlling the pressure, humidity, and temperature in the cabin, the environmental control system makes the system environment in the comfortable range of the human body and ensures that the electronic equipment always works within the allowable temperature range. According to the research, the traditional environmental control system needs a lot of nonpropulsion energy from the engine, and the high-temperature and high-pressure gas produced by the engine compressor is used to drive the environmental control system. At present, in order to use energy more efficiently and economically, further system optimization of the environmental control system has become a research hotspot [1, 2]. At present, there are many methods proposed by researchers but mainly focus on the following two directions:

(1) Continue to drive the environmental control system by bleed air from the engine compressor. Improve the performance of components or use power turbine to replace the traditional air entrainment method, so as to reduce energy waste [3].

(2) By building multielectric or all-electric aircraft, use as much electricity as possible to drive equipment on the aircraft. According to the thermal load and pressure requirements of the cabin, the environmental control system adjusts the motor to control the compressor pressure ratio to obtain the appropriate air supply temperature and pressure. The environment control system with all-electric drive works more stably and the comfort of passengers is improved significantly. At the same time, the all-electric environmental control system does not need to draw air from the engine compressor, so it will not affect the engine performance [4].

In the flight energy-saving design, the overall system optimization is very important because the single subsystem optimization cannot get the optimal solution, so in 2008, the United States launched the integrated aircraft energy technology project [5]. In the INVENT program, the concept of F-35 adaptive power supply and thermal management system (APTMS) was proposed. APTMS improves emissions by using exhaust gas from power turbines and engine compressors. The gas from these engine compressors is directly discharged after expanding and working in the power turbine. The environmental control system driven by

the power turbine was first verified on the F-15 fighter [6, 7]. The original F-15 environmental control system was an open-air circulation refrigeration system, driven by the bleed air from the engine compressor. The main difference between the F-15 and F-35 environmental control systems is the treatment of the gas leaving the power turbine [8]. The gas discharged from the power turbine of F-15 needs to enter the engine room for refrigeration; because of the requirements of the cabin pressure system, the expansion ratio of the power turbine will be relatively small. The power turbine of F-35 directly releases the gas into the external atmosphere and obtains the maximum expansion ratio and power. When the engine compressor bleed parameters are identical, the power turbine of F-35 will output more work.

Adjustable nozzle ring turbines are currently mainly used in variable geometry turbochargers for automobiles. The variable geometry supercharger can continuously adjust the effective flow cross-sectional area of the turbine inlet according to the engine operating conditions, change the turbine inlet airflow parameters, and then change the supercharging pressure, so as to achieve a good match between the supercharger and the engine and also improve the engine transient responsiveness, reducing transient emissions. Compared with the operating characteristics of the variable geometry turbocharger and the traditional supercharger, the former is more efficient and economical in the entire flow range. Improving the adaptability of the turbine under variable operating conditions is a popular direction for the development of turbine technology. However, at present, there are few studies on power turbines using variable nozzle replacement used in aircraft environmental control systems [5]. This paper further studies the dynamic performance of the power turbine in the aircraft environmental control system after the variable nozzle ring is used and the change rule of the variable nozzle ring when the bleed air pressure and temperature change.

2. System Analysis

The environmental control system (Figure 1) in which the power turbine is located is an improved three-wheel high-pressure water removal system (Figure 2) [9]. The environmental control system directly introduces the engine bleed gas into the power turbine, which is directly discharged into the ambient atmosphere after the gas expansion work, and the power turbine directly outputs the shaft work to the turbine compressor assembly [10]. Fresh gas is pumped directly from the surrounding atmosphere by the compressor and supplied to the cabin.

In the traditional environmental control system, after the air is discharged from the engine, the absolute pressure regulator is needed to control the pressure, and the temperature of the future gas passing through the precooler is controlled within a certain range [11]. This process wastes a lot of energy. The environmental control system driven by the power turbine exhausts air directly from the engine, thus eliminating the need for precooler and absolute pressure regulator, which not only realizes the full utilization of energy but also reduces the weight of the system [12].

The bleed pressure and temperature of the engine will change with the flight state. When the bleed state changes, the performance of the power turbine can be controlled by adjusting the opening of the variable nozzle ring, so as to ensure that the output power and torque of the power turbine remain unchanged, so as to isolate the influence of the change of engine operating state on the environmental control system. More importantly, in low altitude or ground operation, because of the low bleed pressure, the system can be operated normally in a larger flight envelope by adjusting the nozzle to obtain a larger starting torque.

This paper calculates the torque, mass flow, and power of the power turbine in the flight curve based on the engine operating parameters of a certain type of flight. When the flight state changes, the torque, mass flow rate, and power change and the adjustment of nozzle opening are calculated. The flight profile used in the calculation is shown in Figure 3.

3. Calculation Model

The blades of the nozzle ring are usually modeled using aerodynamic blades, linear blades, and wing blades. Among them, the pneumatic blade has the largest flow range and the highest aerodynamic efficiency, but the manufacturing process is complex and the blade width is small, which is not conducive to the installation of the rotating shaft [13]. In this paper, NACA0065 symmetric airfoil blades are used in the nozzle ring of the power turbine. The basic parameter model of the power turbine is shown in Table 1, and the three-dimensional model of the turbine and nozzle ring is shown in Figures 4 and 5.

The power turbine uses gas expansion to output torque and power, which drives the load on the shaft to work together. When the turbine is started from a standstill, the torque generated by the gas impact and the friction torque of the bearing must satisfy the following relationship [14]:

$$M_t > M_l, \quad (1)$$

where M_t is the torque of the power turbine and M_l is the drag torque of the system to the turbine.

The rotation equation of the power turbine is

$$I_c \frac{d^2\theta}{dt^2} = \Sigma M_z, \quad (2)$$

where I_c is the total moment of inertia and ΣM_z is the total external torque received by the power turbine, including the gas generating torque and the external load and friction torque.

4. Simulation Parameters

4.1. Simulation Model and Meshing. This article uses ANSYS ICEM software to model and mesh the power turbine in three dimensions. As shown in Figure 6, the model is divided into three parts: a volute, a diffuser, and a blade, and the interface is used as an interface to connect the three models.

In FLUENT, the dynamic numerical simulation of the power turbine is carried out using the sliding grid method.

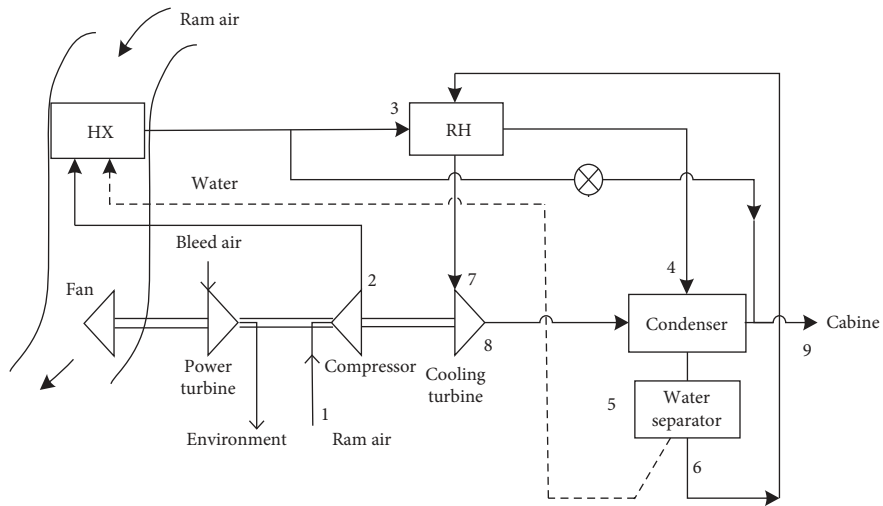


FIGURE 1: Environment control system driven by a power turbine.

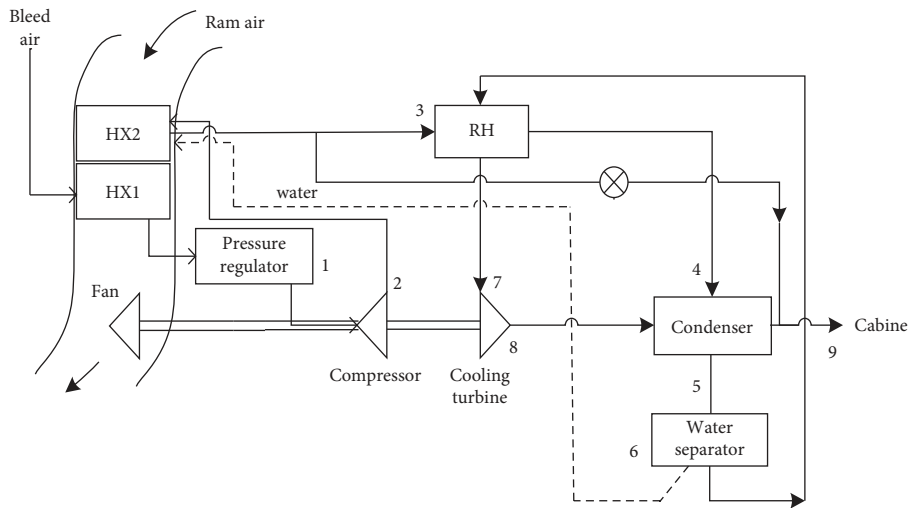


FIGURE 2: Three-wheel boost system.

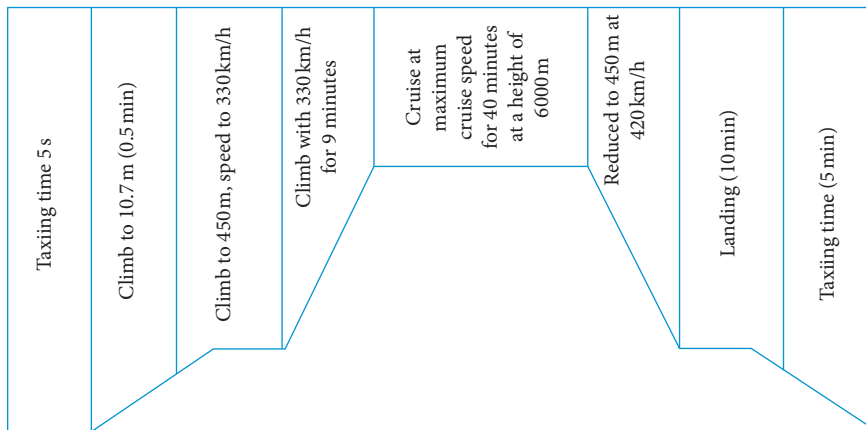


FIGURE 3: Typical mission profile.

TABLE 1: Basic parameters of the power turbine.

Parameter	Value	Parameter	Value
Impeller blade number Z_i	16	Nozzle inner diameter D_{1n}	99
Nozzle ring outlet blade height I_n	5.2	Nozzle throat width b_n	4.5
Impeller outlet hub diameter D_{2h}	24	Impeller exit blade height I_2	14



FIGURE 4: Power turbine.

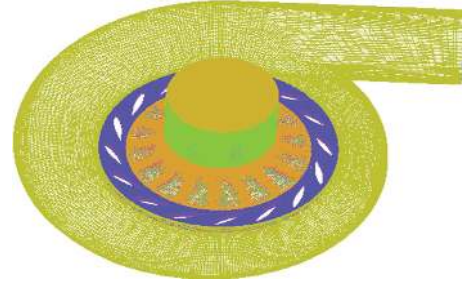


FIGURE 6: Power turbine.

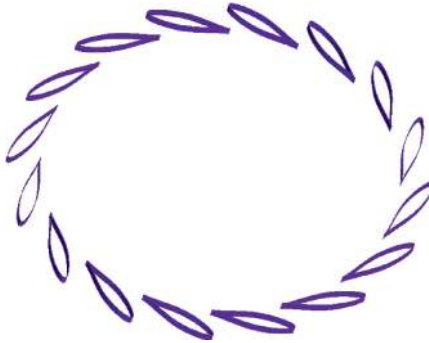


FIGURE 5: Variable area nozzle.



FIGURE 7: Three-dimensional modeling.

In order to obtain better simulation results, the first-order steady-state method is used for calculation, and then it is converted to second-order dynamic calculation after convergence.

The number of power turbine model grids is large, and the convergence speed is slow when using parallel computing in FLUENT. In order to efficiently obtain the performance of the power turbine with different variable nozzle ring openings, the geometric model of the power turbine must be simplified. The common method is to ignore the influence of the intake volute and use the turbine single-flow model to mesh. In this paper, the optimization calculation model uses the 1/4 periodic flow channel model of the power turbine for calculation. 1/4 nozzle ring model and impeller model are selected, and the number of grids is about 700,000 for calculation. The number of corresponding nozzle ring blades in the 1/4 flow channel model is 4 and the number of impeller blades is 4, as shown in Figure 7. Figure 8 is the mesh file inside the runner after the nozzle ring grid and the impeller grid are stitched together. When setting the boundary conditions in FLUENT, the main difference between the 1/4-channel power turbine model and the complete machine model is that the former requires a closed geometric model by adding periodic boundaries in the flow area at the left and right boundaries of the channel. The



FIGURE 8: Grid model.

boundary attribute of the nozzle ring was changed to the pressure inlet, and the definition of the remaining boundary conditions was consistent with the fluent numerical simulation of the whole machine.

4.2. Turbulence Model. The SA model is complete, and the turbulence scale in the model is automatically defined, and no specific flow is required to adjust the closure constant. The effect is better in the prediction of far wake and mixed laminar flow, boundary layer flow, backward step flow and

airfoil flow with small separation. In general, the SA model is more suitable for engineering applications, especially in the airfoil and impeller applications. The SA model is used for calculation in this paper:

$$\begin{aligned} \frac{\partial \tilde{\nu}}{\partial t} &= C_{b1} [1 - f_{t2}] \tilde{S} \tilde{\nu} \\ &+ \frac{1}{\sigma} \left[\nabla \cdot ((\nu + \tilde{\nu}) \nabla \tilde{\nu}) + C_{b2} (\nabla \tilde{\nu})^2 \right] \\ &- \left(C_{w1} f_w - \frac{C_{b1}}{k^2} f_{t2} \right) \left(\frac{\tilde{\nu}}{d} \right)^2 + f_{t1} \Delta U^2. \end{aligned} \quad (3)$$

The turbulent viscosity coefficient μ_T is calculated by the following formula:

$$\mu_T = \rho \tilde{\nu} f_{v1}, \quad (4)$$

$$f_{v1} = \frac{\chi^3}{\chi^3 + C_{v1}^3}, \quad (5)$$

$$\chi = \frac{\tilde{\nu}}{\nu}. \quad (6)$$

ν is the viscosity coefficient of molecular motion and the generated term is

$$\tilde{S} = \Omega + \frac{\tilde{\nu} f_{v2}}{\kappa^2 d^2}, \quad (7)$$

$$f_{v2} = 1 - \frac{\chi}{1 + \chi f_{v1}}, \quad (8)$$

$$\Omega = \sqrt{\left(\frac{\partial w}{\partial y} - \frac{\partial v}{\partial z} \right)^2 + \left(\frac{\partial u}{\partial z} - \frac{\partial w}{\partial x} \right)^2 + \left(\frac{\partial v}{\partial x} - \frac{\partial u}{\partial y} \right)^2}, \quad (9)$$

where Ω is the vorticity.

The function f_w is defined as

$$f_w \equiv g \left[\frac{1 + C_{w3}^6}{g^6 + C_{w3}^6} \right]^{1/6}, \quad (10)$$

$$g = r + C_{w2} (r^6 - r), \quad (11)$$

$$r = \frac{\tilde{\nu}}{\kappa^2 d^2 \tilde{S}}. \quad (12)$$

The function f_{t1} is defined as

$$f_{t1} = C_{t1} g_t \exp \left[-C_{t2} \frac{\omega_t^2}{\Delta U^2} (d^2 + g_t^2 d_t^2) \right], \quad (13)$$

$$g_t = \min \left(0.1 \frac{\Delta U}{\omega_t \Delta x_i} \right), \quad (14)$$

where d is the shortest distance of the solid wall.

The function f_{t2} is defined as

$$f_{t2} = C_{t3} \exp(-C_{t4} \chi^2). \quad (15)$$

Constant values in model equations are

$$\kappa = 0.41,$$

$$C_{b1} = 0.1355,$$

$$C_{b2} = 0.622,$$

$$\sigma = \frac{2}{3},$$

$$C_{v1} = 7.1,$$

$$C_{w1} = 3.239,$$

$$C_{w2} = 0.3,$$

$$C_{w3} = 2,$$

$$C_{t1} = 1,$$

$$C_{t2} = 2,$$

$$C_{t3} = 1.1,$$

$$C_{t4} = 2. \quad (16)$$

4.3. Parameter Settings. Set the nozzle ring installation angle to 12° and the number of nozzle ring blades to 16. The change of the nozzle ring blade opening degree “+” means that the nozzle ring is closed and the flow rate decreases; the nozzle ring blade opening degree change “-” means that the nozzle ring is open and the flow rate increases. There are 7 calculation states of nozzle ring opening: $+10^\circ + 6^\circ + 8^\circ + 3^\circ, 0^\circ, -3^\circ, -6^\circ$, of which 0° is the design state, as shown in Figure 9.

The inlet pressure in FLUENT is set to 3 bar, 3.5 bar, 4 bar, 4.5 bar, and 5 bar and the outlet pressure is set to 1 bar. The starting torque received by the impeller is calculated by udf.

4.4. Grid Independence Verification. Table 2 can be drawn; when the number of grids is 3 million, the calculated value of the turbine efficiency is very different from the calculated value by the number of grids 4 million and 5 million. After the number of grids exceeds 4 million, the increase in the number of grids has little effect on the power turbine efficiency. It is considered that the 4 million grids have reached grid independence.

Using the same data, perform a numerical simulation on the 1/4-channel power turbine model and compare the calculation results with the numerical simulation results of the whole machine as shown in Table 3. It can be seen that the difference between the calculation results of the flow rate and efficiency between the two is very small. In the numerical simulation, the calculation result of the 1/4 flow channel can be approximately used as the numerical simulation result of the power turbine.

4.5. Experimental Program. Figure 10 is a traditional 3-wheel environmental control system, consisting of a turbo compressor, an electric compressor, and a radiator. The pressure

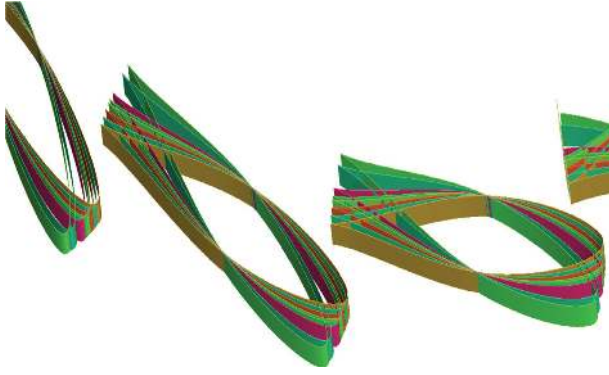


FIGURE 9: Variable nozzle ring.

TABLE 2: Different grid number numerical simulation results.

Number of grids	Mass flow (kg/s)	Expansion ratio	Adiabatic efficiency
3000000	0.2453	3.343	0.8292
4000000	0.2452	3.353	0.8129
5000000	0.2452	3.353	0.8120

TABLE 3: Simulation results of the whole machine and 1/4 flow channel.

Model	Mass flow (kg/s)	Expansion ratio	Adiabatic efficiency
All	0.2452	3.353	0.8129
1/4 flow channel	0.2472	3.301	0.8226



FIGURE 10: Power turbine.

sensor and temperature sensor measure the temperature and pressure of the inlet and outlet of the turbine and compressor and calculate the efficiency of its various components. As shown in Figures 10–13, the high-temperature and high-pressure gas obtained by simulating the engine bleed air is simulated by an electric compressor, and the inlet and outlet temperatures and pressures of the power turbine are measured using pressure sensors and thermocouples, respectively, to calculate the efficiency of the power turbine. The experimental value is compared with the simulation value to verify the rationality of the simulation result [15, 16]. The accuracy of the absolute pressure sensor is 2%, the accuracy of the thermocouple is $\pm 0.5^\circ\text{C}$, the turbine inlet pressure is usually above 200 kPa, the temperature is 30°C – 200°C , the outlet is directly connected to the atmosphere, the pressure is about

100 kPa, and the temperature drop is usually 40°C above. The accuracy of the experimental instrument is sufficient to meet the experimental requirements.

5. Results and Discussion

5.1. Experimental Results. It can be seen from Table 4 that the simulation value is slightly higher than the experimental value by about 5%, which may be because the simulation model does not consider the efficiency reduction caused by the heat conduction of the air introduction pipe and the shell itself. The simulation value and the experimental value are basically consistent, so the aerodynamic force should be basically consistent with the actual situation.

5.2. Simulation Results

5.2.1. Flow Field Analysis. Figures 14–17 are the static pressure distribution of the gas at the nozzle ring blade height of 50% when the nozzle ring blade openings are $+3^\circ$, 0° , -3° , and -6° , respectively. It can be seen from the figure that, in the case of the four middle openings, the low-pressure area obviously appears at the position of the maximum curvature of the suction surface of the blade, and the position of the maximum load of the blade does not change. During the change of the nozzle ring opening from -6° to $+3^\circ$, the pressure value in the center of the low-pressure area is continuously decreasing, which also causes the nozzle ring blade outlet pressure value to continuously decrease, which is consistent with the calculated nozzle ring outlet static pressure data match.

The total pressure cloud at the nozzle ring blade height of 50% is shown in Figures 18–21. It can be seen from the figure that the total pressure loss at the nozzle ring outlet is significantly larger at $+3^\circ$, including 0° , -3° , and -6° . In this case, the total pressure loss is not obvious, and the change of the airflow angle of the nozzle ring blade outlet causes the loss of turbine efficiency.

The Mach number at the nozzle ring blade height of 50% is shown in Figures 22–25. The nozzle ring flow channel is a convergent flow channel. At $+3^\circ$, 0° , and -3° , the suction surface curvature is at the maximum position at the nozzle ring blade height of 50% (low-pressure area). There is a local supersonic area, which is not present at -6° . The presence of a local supersonic zone will affect the uniformity of the flow in the flow field and have a certain effect on turbine efficiency.

When the nozzle ring blade opening is $+3^\circ$, 0° , -3° , and -6° , the impeller blade efficiency distribution is 0.897, 0.900, 0.894, and 0.878, which is consistent with the change trend of turbine efficiency. The static pressure cloud diagram of the long blade of the impeller is shown in Figures 26–29. It can be seen from the figure that there is a significant reverse pressure gradient area at the outlet of the impeller flow channel. As the nozzle ring blades rotate from positive opening to negative opening, the reverse pressure gradient at the outlet of the impeller flow path becomes weaker, and the pressure distribution is more uniform. In the process of changing the opening of the nozzle ring, the decrease in the efficiency of the impeller is much greater than that of the nozzle ring. The main reason is that the opening angle of the nozzle ring blades causes the inlet angle of

TABLE 4: The adiabatic efficiency of the turbine in different states.

Inlet static pressure (kPa)	Inlet static temperature (K)	Expansion ratio	Adiabatic efficiency		Error (%)
			Experimental value	Simulation value	
300	357	4.69	0.72	0.75	4.2
300	312	5.52	0.75	0.79	5.3
410	315	5.27	0.73	0.75	2.7
520	315	6.36	0.81	0.84	3.7



FIGURE 11: Electric compressor.



FIGURE 12: Absolute pressure sensor.



FIGURE 13: Thermocouple.

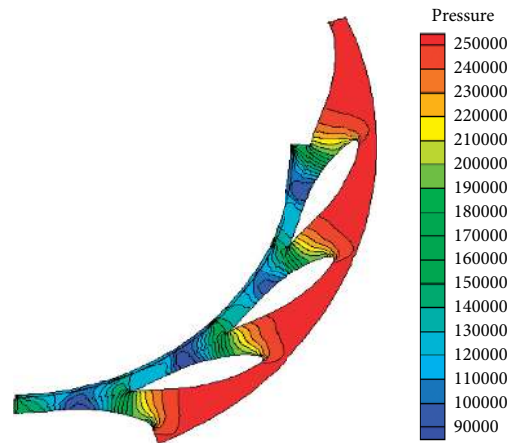


FIGURE 14: Opening +3°.

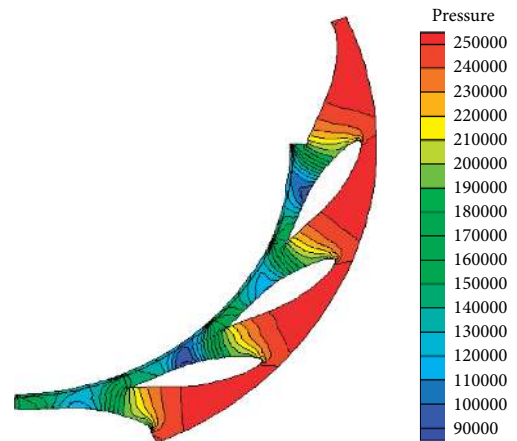


FIGURE 15: Opening 0°.

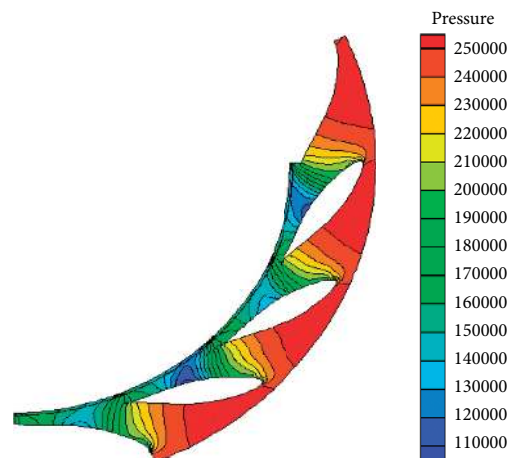
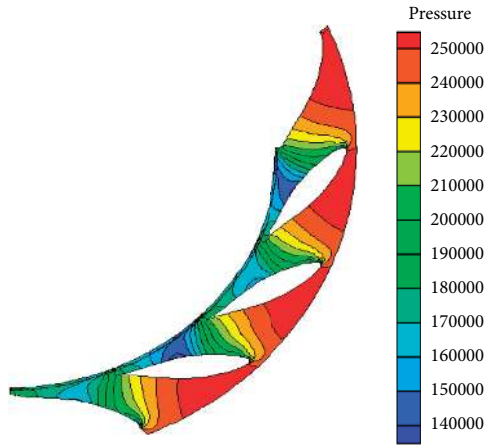
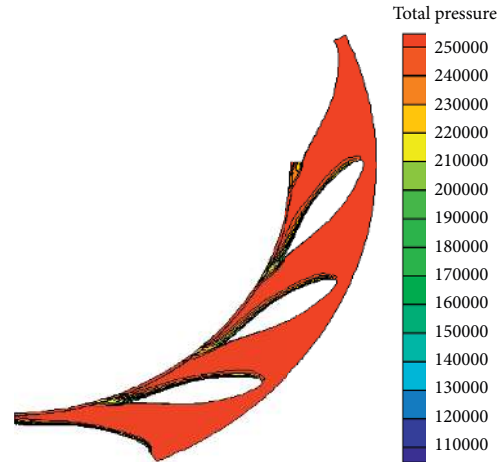
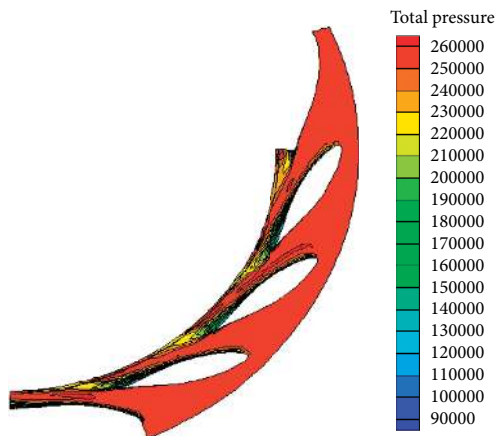
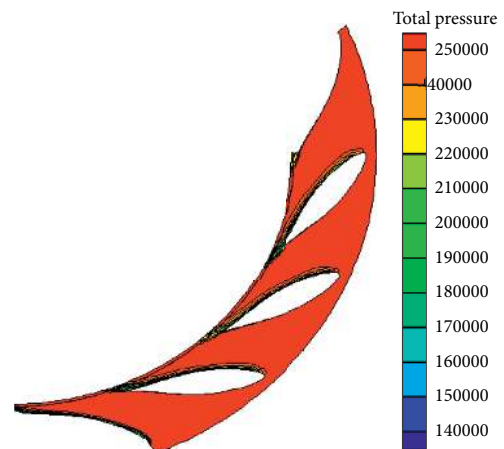
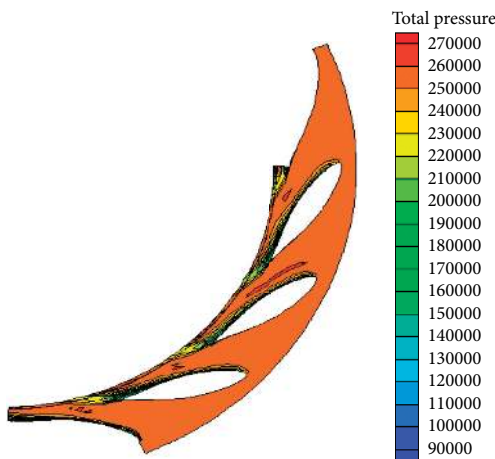
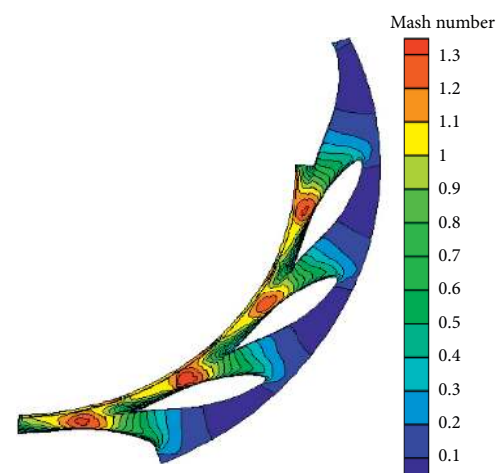


FIGURE 16: Opening -3°.

FIGURE 17: Opening -6° .FIGURE 20: Opening -3° .FIGURE 18: Opening $+3^\circ$.FIGURE 21: Opening -6° .FIGURE 19: Opening 0° .FIGURE 22: Opening $+3^\circ$.

the airflow into the impeller to change significantly and because the nozzle ring blades can rotate, the gap between the nozzle ring and the impeller blades is slightly larger than that of the fixed nozzle ring turbine. The occurrence of divergence is also one of the important reasons for the decrease in the efficiency of the impeller.

5.2.2. Torque. As shown in Figures 30 and 31, when the inlet pressure of the power turbine is low, a larger starting torque can be obtained by opening the opening of the nozzle ring, thereby realizing the purpose of expanding

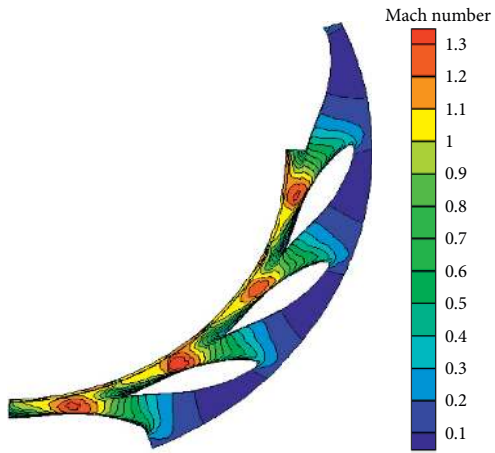


FIGURE 23: Opening 0° .

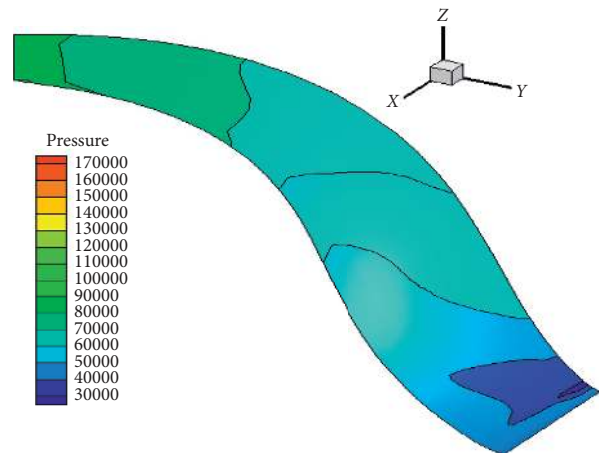


FIGURE 26: Opening $+3^\circ$.

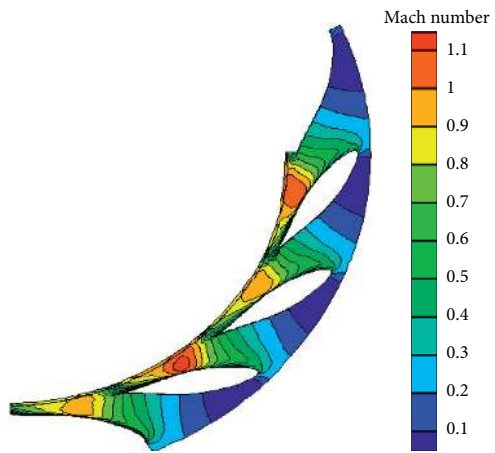


FIGURE 24: Opening -3° .

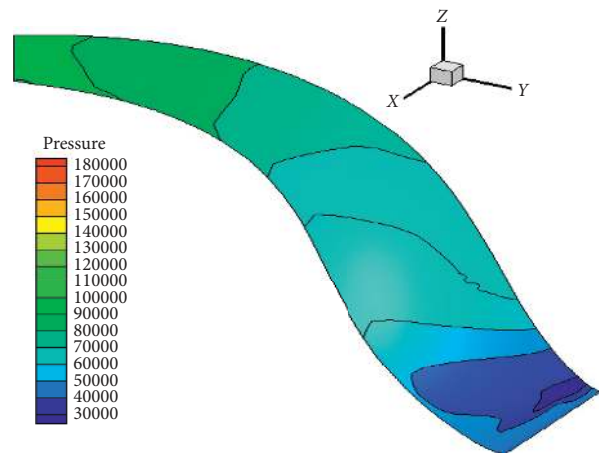


FIGURE 27: Opening 0° .

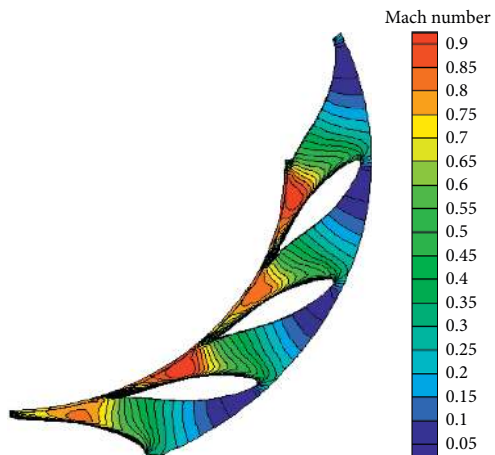


FIGURE 25: Opening -6° .

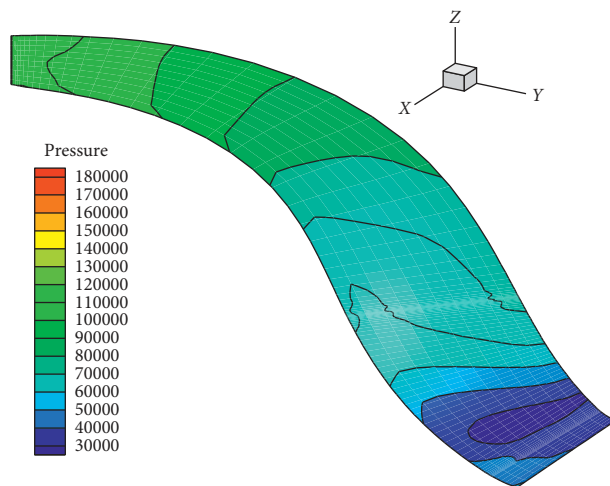


FIGURE 28: Opening -3° .

the operating envelope of the system. Increasing the opening of the nozzle ring expands the system flow rate at the same inlet pressure, thereby obtaining more output torque. When the inlet pressure of the power turbine is too high, the opening of the nozzle ring can be reduced, and the system flow can be reduced, so that the torque

output by the power turbine is unchanged, and the smooth operation of the environmental control system is ensured.

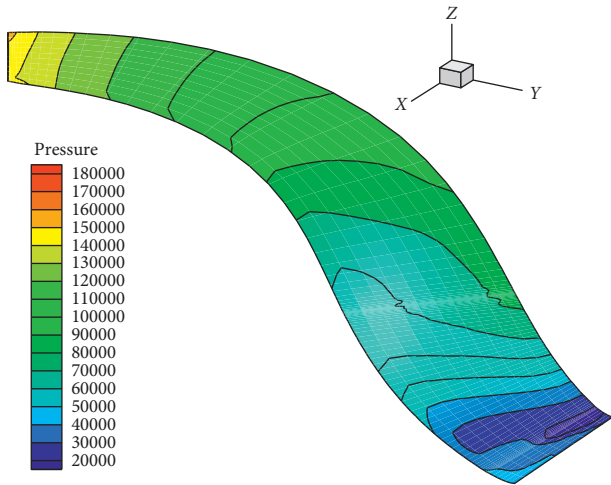


FIGURE 29: Opening -6° .

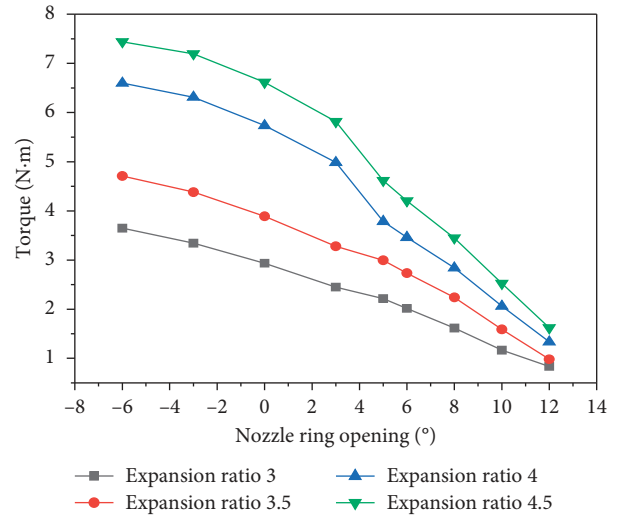


FIGURE 32: Relationship between opening and torque.

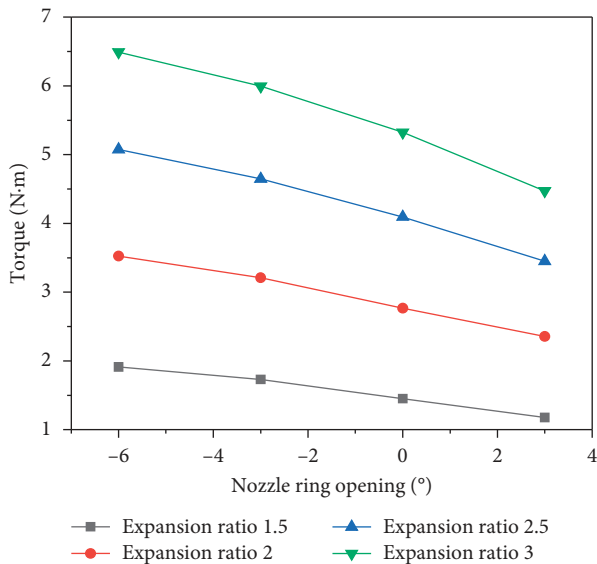


FIGURE 30: Relationship between opening and torque.

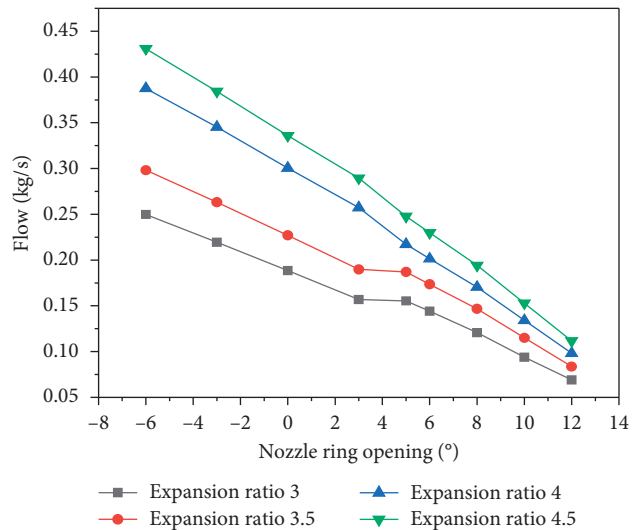


FIGURE 33: Relationship between opening and flow.

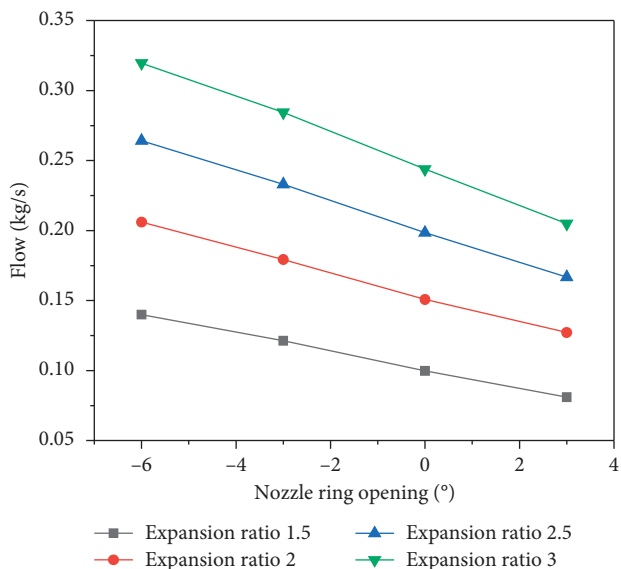


FIGURE 31: Relationship between opening and flow.

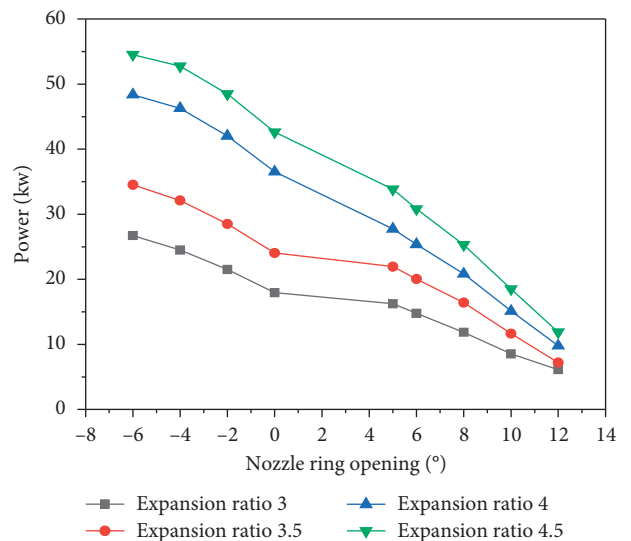


FIGURE 34: Relationship between opening and power.

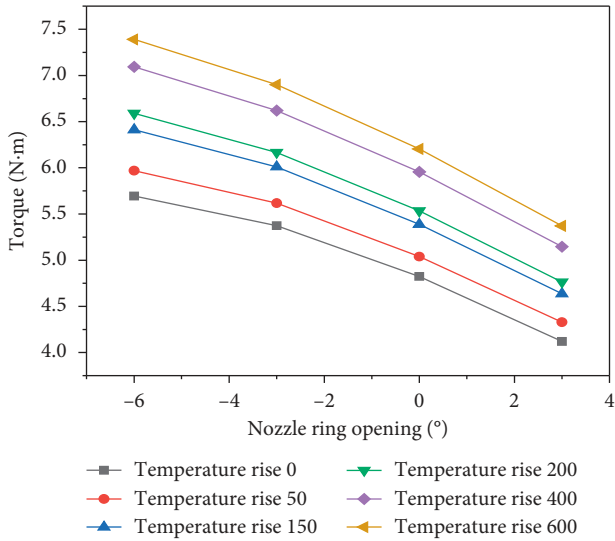


FIGURE 35: Relationship between opening and torque.

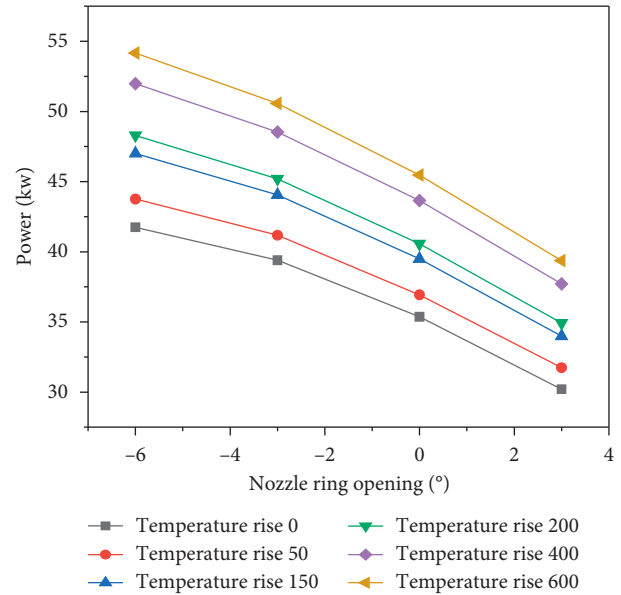


FIGURE 37: Relationship between opening and power.

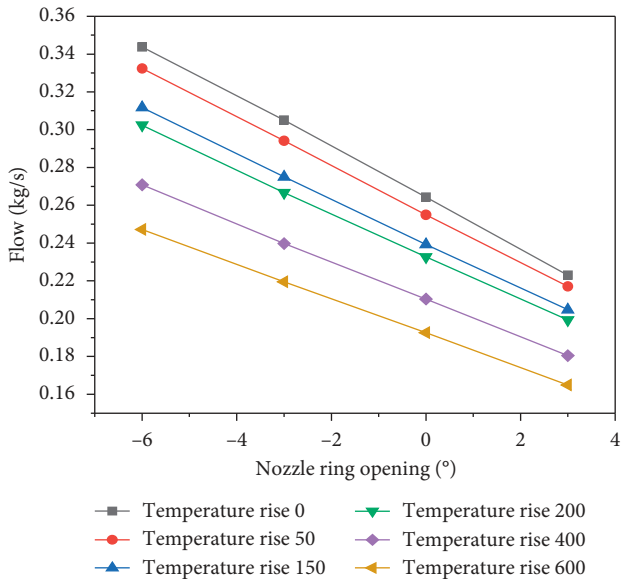


FIGURE 36: Relationship between opening and flow.

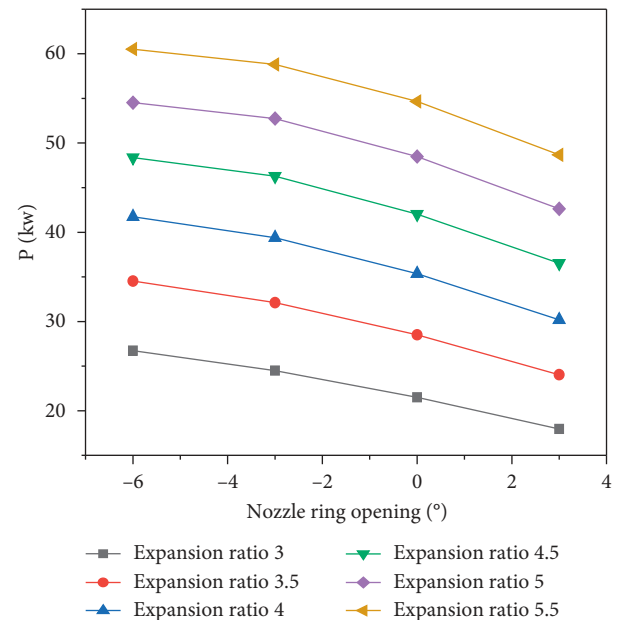


FIGURE 38: Relationship between opening and load.

5.2.3. *Constant Load and Inlet Pressure Change.* As shown in Figures 32–34, when the flight status of the aircraft changes, the bleed air pressure of the engine will change accordingly. If the opening of the nozzle ring is kept unchanged, the power and torque output by the power turbine will also change accordingly. In order to maintain the stable operation of the environmental control system, the output power and torque of the power turbine can be adjusted by increasing or decreasing the opening of the variable nozzle ring.

5.2.4. *Constant Load Change and the Inlet Temperature Changes.* As shown in Figures 35–37, when the inlet temperature of the power turbine changes, adjusting the opening of the variable nozzle can reduce the output power to match the load, thereby reducing the impact of the change in the engine bleed state on the environmental control system.

5.2.5. *Load Change and the Inlet Constant.* As shown in Figure 38, when the nozzle ring opening is changed from +0 to +6, the power can be increased by 25%, 21%, 18.1%, 15%, 12.4%, and 12.9%. When the nozzle ring opening is changed from +0 to -3, the power can be reduced by 16.5%, 15.7%, 15%, 13%, 12.1%, and 10.9%.

6. Conclusion

The power turbine with an adjustable nozzle ring structure can control the amount of engine bleed air according to the power required by the environmental control system. According to the flight profile, the calculated air intake of the

power turbine is significantly smaller than that of the existing aircraft environmental control system. In addition, the environmental control system can be started at a lower bleed pressure, which expands the operating envelope of the system. Therefore, a power turbine with an adjustable nozzle ring structure has the following characteristics. (1) The air circulation system driven by a power turbine with an adjustable nozzle ring structure can freely adjust the amount of bleed air according to the load, reduce fuel compensation, and realize the full use of energy. (2) The opening of the turbine nozzle can be increased or decreased to reduce the starting pressure of the power turbine and expand the range of use of the environmental control system. (3) And through the numerical simulation of the power turbine, it can be concluded that by adjusting the variable nozzle ring blades, the power turbine can provide sufficient work for the compressor throughout the flight. And when the temperature and pressure of the bleed air change, the opening can be adjusted to make the environmental control system run smoothly. In this way, the impact of changes in the engine bleed air parameters on the environmental control system is isolated.

In this paper, the gap between the nozzle ring blade and the turbine casing and the rotation axis of the nozzle ring blade are ignored in the calculation simulation. These gaps have a significant impact on turbine performance, are an important part of turbine energy loss, and also have an impact on torque. All should be considered. It is also possible to conduct research on the variable nozzle ring control actuator of the power turbine, as well as the control law of the variable nozzle ring and how to match the power turbine and the ring control system better and faster. In this paper, the research on the air circulation system driven by a power turbine with a variable nozzle ring is in its infancy, and there are still many problems to be studied in the future.

Data Availability

The turbine's data used to support the findings of this study are included within the article. The environmental control system data used to support the findings of this study are available from the corresponding author upon request.

Conflicts of Interest

The authors declare that there are no conflicts of interest regarding the publication of this paper.

Acknowledgments

This work was supported by the corresponding author Dalin Zhang.

References

- [1] X. Su, F. Xu, and H. Ang, "Present status and future of aircraft environment control system," *Aeronautical Manufacturing Technology*, no. 10, pp. 40–46, 2002.
- [2] X. Yuan, "Developing trend discussion of control systems of high performance military aircraft," *Acta Aeronautica et Astronautica Sinica*, no. S1, pp. 2–4, 1999.
- [3] Q. Lu, D. Zhang, and S. Xiao, "Performance analysis of the power turbine in a environmental control system," in *Proceedings of the CSAA/IET International Conference on Aircraft Utility Systems (AUS 2018)*, Guiyang, China, June 2018.
- [4] R. A. Roberts and D. D. Decker, "Control architecture study focused on energy savings of an aircraft thermal management system," *Journal of Dynamic Systems, Measurement, and Control*, vol. 136, no. 4, Article ID 041003, 2014.
- [5] P. Abolmoali, J. A. Parrilla, and A. Hamed, "Integrated aircraft thermal management & power generation: Reconfiguration of a closed loop air cycle system as a Brayton cycle gas generator to support auxiliary electric power generation," SAE, Warrendale, PA, USA, Technical Paper 2014-01-2192, 2014.
- [6] S. Rajoo and R. Martinez-Botas, "Variable geometry mixed flow turbine for turbochargers: An experimental study," *International Journal of Fluid Machinery and Systems*, vol. 1, no. 1, pp. 155–168, 2008.
- [7] A. Simpson, S. Spence, and J. Watterson, "Numerical and experimental study of the performance effects of varying vaneless space and vane solidity in radial inflow turbine stators," in *Proceedings of the American Society of Mechanical Engineers (ASME)*, pp. 1495–1505, Washington, DC, USA, 2008.
- [8] D. Matullch, "High-temperature bootstrap compared with F15 growth air cycle air conditioning system," SAE, Warrendale, PA, USA, Technical Paper 891436, 1989.
- [9] F. Couaillac, "Environmental control systems for the all-electric aircraft," M.S. thesis, Cranfield University, Cranfield, UK, 2007.
- [10] S. Yu and E. Ganev, "Next generation power and thermal management system," SAE, Warrendale, PA, USA, Technical Paper 2008-01-2934, 2008.
- [11] S. Fu, Y. Zheng, K. Kan et al., "Numerical simulation and experimental study of transient characteristics in an axial flow pump during start-up," *Renewable Energy*, p. 146, 2019.
- [12] C. Liu, "Proceedings of the institution of mechanical engineers, Part I," *Journal of Systems and Control Engineering*, vol. 5, 2020.
- [13] D. Bender, "Integration of exergy analysis into model-based design and evaluation of aircraft environmental control systems," *Energy*, vol. 137, no. 15, pp. 739–751, 2017.
- [14] J. O. Gray and C. G. Downes, "A formal computer based design environment for aircraft engine control systems," *Computer Aided Design in Control Systems 1988*, vol. 21, no. 8, pp. 431–439, 1989.
- [15] J. Eichler, "Simulation study of an aircraft's environmental control system dynamic response," *Journal of Aircraft*, vol. 12, no. 10, 2012.
- [16] S. Yang, S. Chen, X. Chen, X. Zhang, and Y. Hou, "Study on the coupling performance of a turboexpander compressor applied in cryogenic reverse Brayton air refrigerator," *Energy Conversion*, vol. 122, 2016.